Influence of the cooling rate below Ms on the martensitic transformation in a low alloy medium-carbon steel

Jia-Hong Liu, N. Binot, Denis Delagnes, M. Jahazi

Available online at www.sciencedirect.com

jmr&t Journal of Materials Research and Technology

journal homepage: www.elsevier.com/locate/jmrt

Original Article

Influence of the cooling rate below Ms on the martensitic transformation in a low alloy medium-carbon steel

J.H. Liu [a,*], N. Binot [b], D. Delagnes [c], M. Jahazi [a]

[a] Mechanical Engineering Department, École de technologie supérieure, 1100 Rue Notre-Dame Ouest, Montreal, H3C 1K3, QC, Canada

[b] Materials and Processes Laboratory, Safran Landing Systems, Etablissement de Bidos, 64400, Oloron-Sainte-Marie, France

[c] Institut Clément Ader (ICA), Université de Toulouse, CNRS, IMT Mines Albi, UPS, INSA, ISAE-SUPAERO, Campus Jarlard, 81013, Albi CT, Cedex 09, France

ARTICLE INFO

Article history:
Received 12 January 2021
Accepted 19 February 2021
Available online 25 February 2021

Keywords:
Kinetics
Modeling
Martensitic phase transformation
Dilatometry

ABSTRACT

The influence of cooling rate *below* the martensite start temperature, M_s, on the kinetics of martensitic transformation in a medium carbon low alloy steel was determined using high resolution dilatometry, optical microscopy and X-ray diffraction techniques. A two-stage transformation was observed for slow cooling rates while at higher cooling rates, martensitic transformation occured through a single stage process. It is shown that the Koistinen–Marburger equation cannot adequately describe the observed two-stage transformation. A new equation is proposed in order to model the evolution of martensitic transformation by considering the influence of post M_s cooling rate. The method considers contributions from both, the initial austenite and the carbon enriched austenite. The underlying mechanisms are discussed and validated with experimental findings.

1. Introduction

Martensitic transformation is generally depicted as a diffusionless mechanism that is solely defined by the degree of undercooling which takes place upon reaching the martensite start temperature (M_s) during a quench [1,2]. A sufficiently fast cooling rate is necessary in order to avoid the formation of intermediate phases such as bainite. The conventional method of carrying quench experiments is by dilatometry using constant cooling rates from the austenitization to room temperature [3,4]. The dilatometric data is then used to construct continuous cooling rate diagrams and to model the evolution of the martensitic fraction as a function of temperature via the Koistinen–Marburger (K-M) equation [4,5]. However, such experiments and modeling with K-M equation without considering the duration required to reach from M_s to the martensite finish temperature (M_f) could be an over simplification for industrial applications. In fact, as quenching

* *Corresponding author.*
E-mail address: jia-hong.liu.1@ens.etsmtl.ca (J.H. Liu).

https://doi.org/10.1016/j.jmrt.2021.02.075

is generally an uncontrolled process, variable cooling rates are observed throughout the process particularly, in the case of large size components. As the temperature decreases, the cooling rate is significantly reduced due to the small temperature differences between the component and the quenching medium. The process could then take several hours before the component actually reaches room temperature, lingering around the transformation range. Using a constant cooling rate from austenitization to room temperature to determine the kinetics of phase transformation could, therefore, lead to inaccurate estimations of phase changes. By using various cooling rates under M_s, it will be possible to better understand the effect of time on martensitic transformation and provide a more accurate representation of the quenching process. Such understanding is of critical importance when it comes to developing numerical models for predicting quench induced distortion of large size components with complex geometries made of medium carbon steels.

Knowing the kinetics of phase transformation is of great importance by allowing the development of models which provide means for engineers to predict and design materials accordingly. Dilatometry has become a necessary tool in the study of phase transformation. Researchers have used the dilatometry with the combination of optical and electron microscopy and synchrotron X-ray diffraction to determine the microconstituent fractions [6]. Others have used dilatometry coupled with synchrotron X-ray diffraction to study the kinetics of austenite reversion and its stability [7–9].

In the simplest form, the kinetics of martensite transformation are often obtained by relating the length change of the sample during the dilatometry test to the progress of martensite transformation. The standard reverse S shape is usually observed when using a constant cooling rate from austenitization to room temperature [10–12]. However, some researchers have observed “unusual” [13] and “abnormal” [14] kinetics in which irregularities have been noticed on the dilatometry curves during the martensitic transformation. These variations in the fractions of formed martensite as a function of temperature have the particularity of occurring in the form of steps interpreted as the acceleration or deceleration of the transformation. The steps are easily discernable as peaks when the results are plotted with the first derivative, representing the rate of transformation. Loewy et al. [13] related such observations to the simultaneous formation of martensite blocks in different packets. Furthermore, they reported that the overall transformation rate was independent from the employed cooling rates. Villa et al. [14] described the anomalous deceleration martensite formation as the effect of strain and interfacial energy while the acceleration was related to the autocatalytic nucleation of martensite. Liu et al. [15], associated the splitting behavior of martensitic transformation to the precipitation M_3C particles. Although some studies report unusual behavior in dilatometry diagrams, most studies focus mainly on the athermal aspect of the transformation and very little attention has been paid to the influence of post M_s cooling rates on the transformation.

In the present work the influence of cooling rate (i.e. the time factor) between M_s and M_f on the evolution of martensitic transformation was investigated. A new equation is proposed that more accurately describes changes in martensite fraction during the quench process.

2. Experimental procedures

The studied material is a wrought low alloy medium-carbon steel, with the following chemical composition: Fe–0.43C-0.71Mn–0.006P–0.001S–1.63Si–1.81Ni–0.83Cr–0.40Mo–0.07-V–0.11Cu (wt. %). Dilatometric experiments were carried out using the high resolution Bähr DIL 805A/D dilatometer with samples of 4 mm in diameter and 10 mm in length, extracted from the as received material. Details of the applied thermal cycles are shown in Fig. 1. The colored lines represent the different cooling rates after the M_s temperature. All samples were heated from room temperature to 878 °C with the same heating rate of 1.42 °C/s and then soaked for 600 s, both under vacuum. The samples were then cooled using helium with an identical cooling rate of −2.27 °C/s until 300 °C. The temperature of 300 °C was determined based on preliminary dilatometry tests that showed this temperature is slightly above the actual M_s. Subsequent cooling rates of −2.27 °C/s, −0.33 °C/s, −0.16 °C/s and −0.11 °C/s were then used to study the effect of cooling rates below M_s on the kinetics of martensitic transformation. For easier reading purposes, these cooling rates will be henceforth labeled as CR1, CR2, CR3 and CR4, as also indicated in the inset of Fig. 1.

Following the dilatometry experiments, the samples were cut in half for microstructural investigations. Each sample were manually ground to P4000 SiC grit paper and finished by polishing down to 1 μm with a diamond solution. The samples were then etched using a 3% Nital solution for 7 s at room temperature. Optical micrographs are acquired using a laser scanning confocal microscope, Olympus LEXT OLS4100.

The others halves of the cut dilatometry samples are also used for quantitative X-ray diffraction (XRD) tests in order to determine the amount of retained austenite (RA).

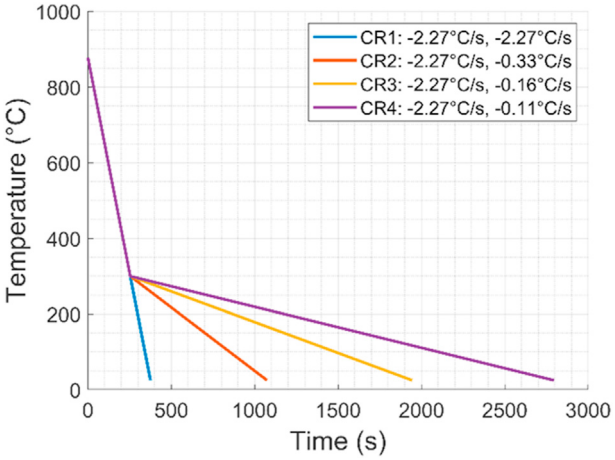

Fig. 1 – Planned thermal cooling cycles in which they share an initial and identical cooling rate of −2.27 °C/s until the temperature of 300 °C. It is then followed by cooling rates of −2.27 °C/s, −0.33 °C/s, −0.16 °C/s and −0.11 °C/s for the color blue, red, orange and purple, respectively.

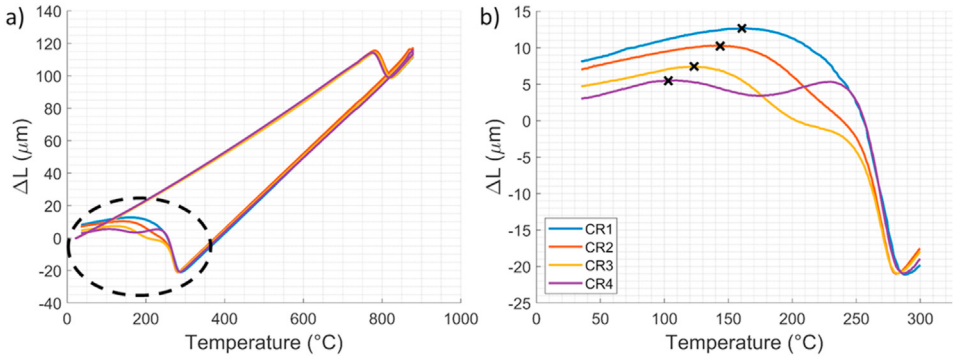

Fig. 2 – (a) Complete dilatation curves for all four investigated thermal cycles. (b) Enlarged area corresponding to the martensitic transformation (dashed circle in Fig. 2(a)).

Measurements were performed with a Malvern Panalytical's X'Pert^3 MRD diffractometer with Co K-α radiation under a current of 40 mA and a voltage of 45 kV. A 2θ scan range of 48°–108° with a scanning speed of 1.3°/min was used. The software HighScore was used for background removal as well as identification of the peaks' position. The volume fraction of RA was then calculated using XRD peak intensities following the Ref. [16].

3. Results

Fig. 2(a) shows the complete dilatation curves as a function of temperature during martensitic transformation for all four investigated cooling rates. An enlarged area of the transformation, indicated by a dashed circle, is shown in Fig. 2(b). As observed, the kinetics of martensite transformation show different patterns with decreasing cooling rates. Specifically, for CR1, a conventional dilatation rate is identified where a strong and initial phase transformation is observed as soon as the temperature reaches the M_s and gradually slows down as the remaining austenite is transformed. Transformation stops when the dilatation curve follows a straight line. However, for CR2, CR3 and CR4, discontinuities, in the form of acceleration and deceleration of transformation, can be observed. This behavior is consistent with previous findings from other researchers [13,14,17]; however, they were not associated with the cooling rates below M_s. It is interesting to note that the martensite fraction formed during the first stage does not solely decrease when lower cooling rates are used. In fact, for CR4 with a slower cooling rate than CR3, the observed fraction formed before the deceleration is higher than for CR3, which suggests the presence of an inflection point. The black crosses in Fig. 2(b) indicate the local maxima used as estimations of the M_f. The measured maxima values are 163 °C, 151 °C, 131 °C and 117 °C for CR1, CR2, CR3 and CR4, respectively. The above finding reveals that as the cooling rate below M_s becomes lower the microstructure becomes more and more stable and the M_f is nearly reached. It must be mentioned that due to mechanical stabilisation of retained austenite a complete transformation (i.e., 100%) of austenite to martensite is not expected, unless reaching very low temperatures and therefore accurate determination of M_f is more challenging [18,19]. It was also found that the final length of the sample decreased with the cooling rate. These length differences could be attributed to the stabilization of austenite due to carbon partitioning from supersaturated martensite [10]. Consequently, the length differences could provide an indication for the

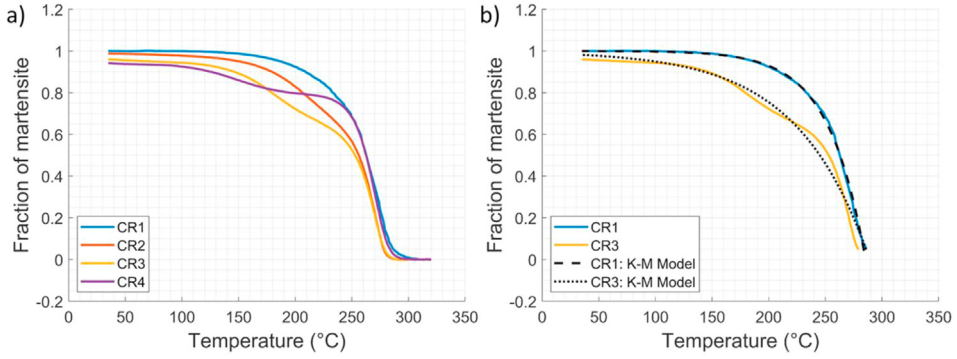

Fig. 3 – (a) Martensite fractions as a function of temperature calculated from dilatation curves. The final fraction achievable for CR2, CR3 and CR4 is determined with the assumption that CR1 forms a fully martensitic steel. (b) Modeling of the transformation kinetics using the K-M equation.

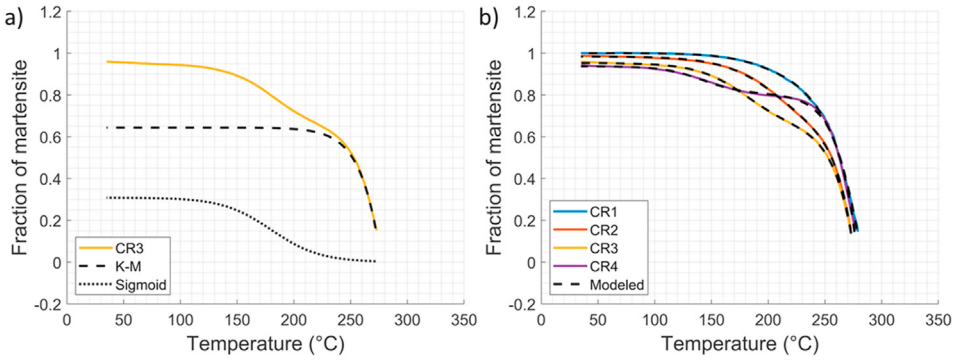

Fig. 4 – (a) Representation of the modeling method of CR3 by the decomposition of the proposed equation into both sub-equations. (b) Modeling of martensite transformation kinetics using the newly proposed equation with the least squares method.

amount of RA at room temperature. The relation between the cooling rate and the amount of RA will be presented and discussed in the upcoming sections of this paper. The calculated RA from dilatometry will also be compared to the experimentally measured RA by XRD to validate this hypothesis.

Further analysis of the results was conducted by using the lever rule to convert the dilatation curves into transformed phase fractions. For the incorporation of the length differences in the determination of RA, an initial known value of martensite fraction is needed from the set dilatometry of curves. However, such value is impossible to obtain based solely on dilatometry. Therefore, at this preliminary stage, without any additional information regarding the microstructure, it is assumed that CR1 results in a fully martensitic microstructure. This allows the determination of RA for the other curves in terms of proportions. The amount of RA for CR2, CR3 and CR4 due to the final length differences in comparison to CR1 was estimated using the following equation:

$$X_i = \frac{\Delta L(T)_{CRi} - \Delta L(T)_{A,\ CRi}}{\Delta L(T)_{M,\ CR1} - \Delta L(T)_{A,\ CRi}}$$

where X_i represents the calculated fraction of martensite for dilatation curve i, and CRi is the corresponding cooling rate. A and M represent the phase austenite and martensite, respectively. For instance, $\Delta L(T)_{A,\ CRi\ |\ i=3}$ is the change in length for the austenite phase from the dilatation curve of CR3, at temperature T. Calculated fractions derived from dilatation curves are reported in Fig. 3(a). It can be seen that for CR1 the transformation kinetics represents a reverse S shape. However, as the cooling rate decreases the sharpness of the shape gradually fades away and a double reverse S shape is observed.

Table 1 – Values of the proposed equation's parameters.

Cooling Cycle	F	A	$\Omega 1$ (K^{-1})	$\Omega 2$ (K^{-1})	CM_s1 (°C)	CM_s2 (°C)
CR1	1	0.942	0.035	0.078	282.8	246.8
CR2	0.984	0.598	0.073	0.040	276.0	209.6
CR3	0.953	0.676	0.068	0.046	276.9	179.3
CR4	0.937	0.861	0.058	0.063	279.3	137.2

A common practice is to model the martensitic phase transformation as a function of temperature using the K-M equation [20]:

$$X = 1 - \exp[-\Omega\ (CM_s - T)]$$

where X is the calculated fraction of martensite, Ω is a transformation rate parameter, CM_s the calculated M_s temperature and T the temperature. Variants of this equation have also been devised in order to incorporate the amount of remaining austenite available to transform and a better description of the onset of transformation [21,22]. As expected, due to the high cooling rate of CR1, K-M is able to accurately predict the martensitic transformation with $\Omega = 0.031\ K^{-1}$ and $CM_s = 284.3$ °C. However, with CR3, K-M equation cannot describe the second stage of transformation as shown in Fig. 3(b). Only CR3 was shown here in order to alleviate the graph. It is clearly visible that modeling CR2 and CR4 with K-M equation will also result in a poor agreement.

The above findings clearly reveal the presence of a two-stage transformation process when the cooling rate below M_s is changed. This phenomenon is formalized in the form of an addition of a second term to the conventional K-M equation:

$$X = F\left(A\ \{1 - \exp[-\Omega 1\ (CM_s 1 - T)]\} + (1 - A)\left\{\frac{1}{1 + \exp[-\Omega 2\ (CM_s 2 - T)]}\right\}\right)$$

where F indicates the maximum fraction of martensite transformed and A, the fraction by either sub-equations with both having values between 0 and 1. The parameters $\Omega 1$ and $\Omega 2$ represent the transformation rate for each stage. Lastly CM_s1 and CM_s2 are the calculated martensite start temperatures.

The rationale behind the proposed equation is illustrated in Fig. 4(a). The equation is decomposed and both sub-equations are plotted separately with the dashed line representing conventional K-M equation and the dotted line, the new term. Again, only CR3 is shown for the sake of simplicity. This second term from the equation corresponds to the transformation of the second stage and takes the form of a general sigmoid equation. The proposed equation considers the transformation as a sum of two consecutive

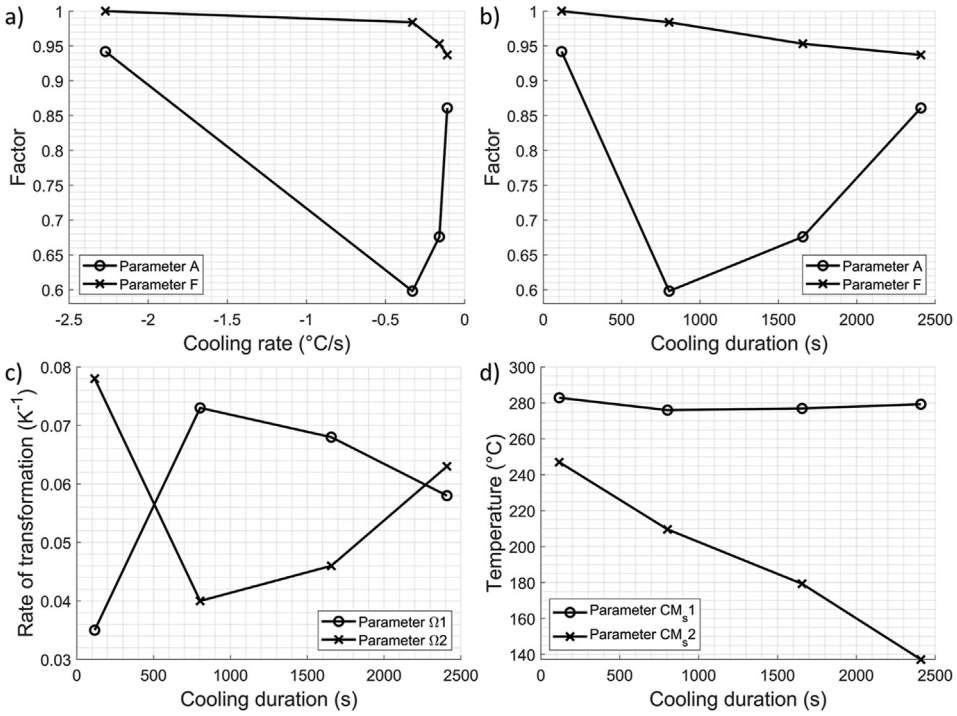

Fig. 5 – (a) Evolution of parameters A and F as a function of cooling rates. (b–d) Evolution of parameters, A, F, $\Omega 1$, $\Omega 2$, CM_s1 and CM_s2 as a function of cooling durations for the temperature range of 300 °C to room temperature. Values are extracted from experimental data using the proposed equation.

transformation. Similarly to the parameters from the K-M equation, the rate of transformation ($\Omega 2$) and start of the transformation (CM_s2) of the second stage are needed. The extraction of these parameters provides information regarding the kinetics of transformation for the second stage. For instance, a higher value of $\Omega 2$ means the transformation occurs at a higher rate.

The fractions contributed by each sub-equation were determined by the product of F with A and 1-A which, once added, gives the global fraction. A similar method was also proposed with the use of two K-M equations in Ref. [23]. The main difference is that with a two K-M equations approach, two separate boundary conditions are needed in order to limit the application of each equation. Otherwise, negative phase fractions could be obtained, which are physically improbable. By introducing the sigmoid equation, as a second sub-equation, the above limitation is suppressed once the initial martensitic transformation has initiated. Thus, in the present approach, K-M will always be used to model the first stage of transformation while the second term ensures the proper modeling of the second stage, if it is present. In such cases, it is expected that $CM_s1 > CM_s2$.

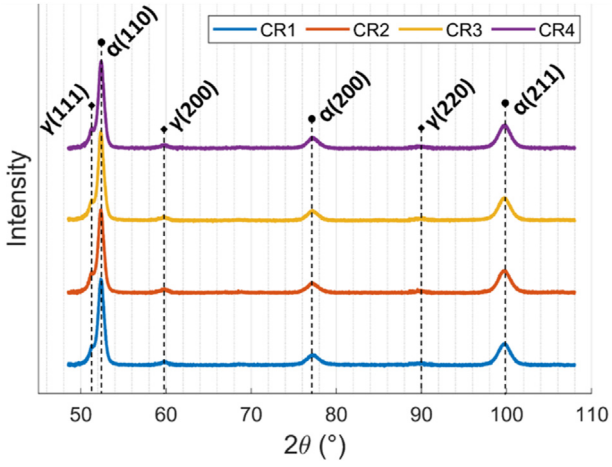

Fig. 6 – Retained austenite peaks for a 2θ scanning range of 48°–108°.

The values of the parameters in the new model for the present paper are reported in Table 1. As previously discussed, the parameter F, representing the maximum attainable phase fraction, progressively decreases with slower cooling rates. When plotted as a function of cooling rate, it is hardly possible to distinguish a trend, as shown in Fig. 5(a). However, as shown in Fig. 5(b-d) when the parameters are plotted against the cooling durations, the influence of the cooling rate is better visualized and if any relation exists, it can be easily extracted and modeled, providing parameters that are now time dependent. By implementing these time dependent parameters in the proposed equation, it indirectly provides the kinetics of martensitic transformation. The durations correspond to the time required to cool from 300 °C to room temperature, depending on the applied cooling rate. As for A, $\Omega 1$ and $\Omega 2$, a more parabolic evolution is observed. This is also expected due to the presence of an inflection point, as previously mentioned. Thus, the inflection point would be somewhere between CR2 and CR3 where the maximum or

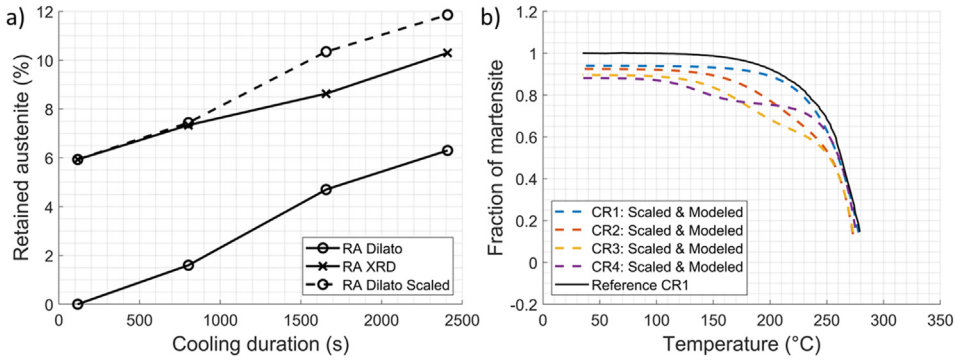

Fig. 7 – (a) Retained austenite as a function of cooling durations. The initial assumption of a fully martensitic steel for CR1 is corrected and to the measured values from XRD. (b) Modeling of martensite transformation kinetics using corrected values of the parameter *F*.

minimum is located. For CM_s1, the values vary from 276.6 to 283.8 °C. As for CM_s2, it decreases considerably from 246.8 to 137.2 °C in an almost linear fashion.

The amount of RA is deduced from XRD measurements and used to complement the modeling previously performed from the dilatometry results. Within the full range of 2θ angle shown in Fig. 6, a total of 6 peaks were identified which provides a higher accuracy regarding the determination of the volume fraction of RA at room temperature. The volume fractions derived from these peaks are 5.93%, 7.34%, 8.63% and 10.3% for CR1, CR2, CR3 and CR4, respectively. As expected, the volume fractions clearly increase with a slower cooling rate below M_s or with a longer cooling duration.

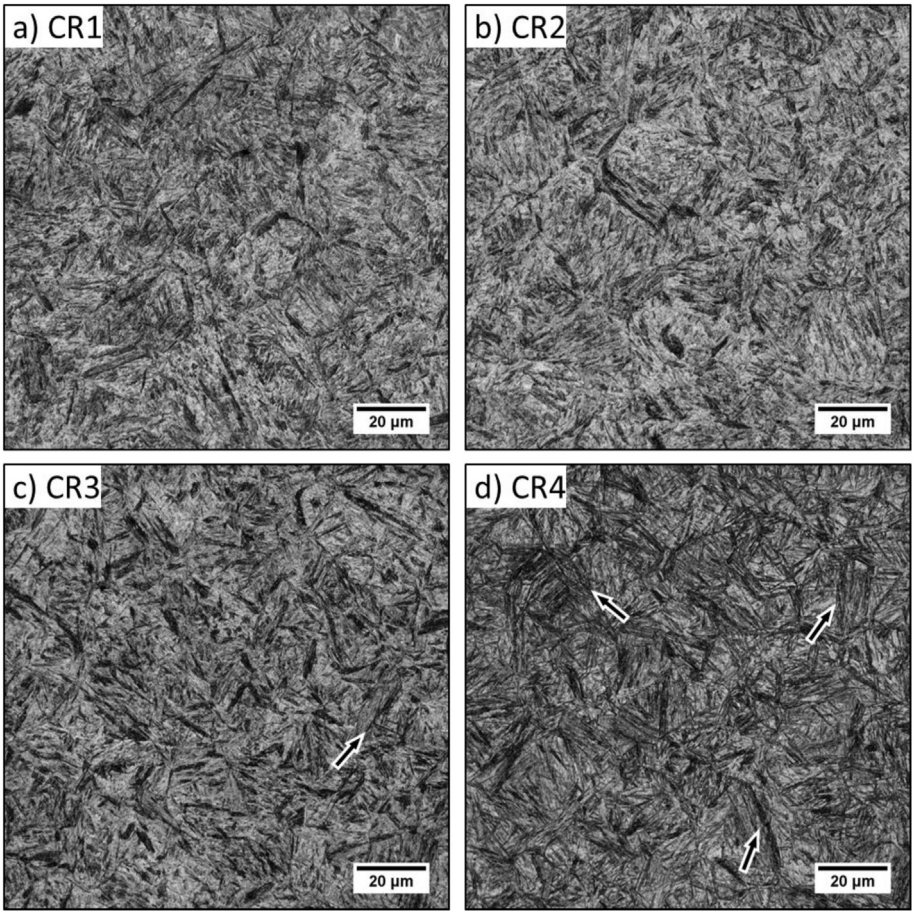

Fig. 8 – Optical micrographs of martensitic microstructures corresponding to each dilatometry sample. (a–b) A similar microstructure consisting of martensite laths is obtained. (c–d) An increasing number needle-like microstructure is observed.

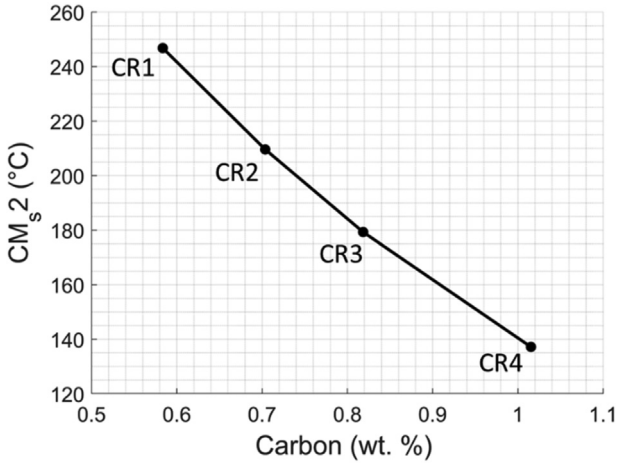

Fig. 9 – Decrease of the calculated martensite start temperatures for the second phase transformation due to the increase of carbon concentation in the remaining austenite during transformation.

It was previously considered that the microstructure of CR1 is fully martensitic. Such assumption was useful in order to assess phase proportions based on length differences without any known measurement of the initial RA. However, now that a RA volume fraction of 5.93% has been measured, the initial assumption should be corrected. This new value from XRD was implemented for CR1, and the subsequent values from dilatometry are recalculated and rescaled by maintaining their proportions from the length difference. A total of 7.44%, 10.35% and 11.86% for CR2, CR3 and CR4 is calculated based on the new value of CR1. Fig. 7(a) shows the evolution of the amount of RA as a function of the cooling duration. The full line with circles show the calculated austenite from the final length differences measured by dilatometry experiments whereas the full line with crosses is the RA derived from the analysis of the diffraction peaks. As for the dash line with circle, it is the RA from dilatation scaled to the same initial value of XRD.

Visually, both methods display a very similar trend. Although there is some discrepancies in values for CR3 and CR4 between both methods, the approximation of the amount of RA using the final length difference is still plausible. However, with this approach, only proportions can be estimated between dilatation curves if the initial RA is unknown.

With more precise values with retained austenite available, the modeling of the martensitic transformation from the proposed equation only requires changing the parameter F, corresponding to the maximum fractions of martensite. Fig. 7(b) shows the final modeling with values for the parameter F of 0.941, 0.923, 0.897 and 0.881.

Fig. 8 shows optical micrographs of each dilatometry sample which are acquired in order to investigate the main mechanism responsible for the two-stage transformation as well as provide valuable insights of its effect on the microstructure. As expected, the main product formed consists of martensite. However, there's a noticeable difference in the microstructures as the cooling rate below M_s slows down from CR1 to CR4. As shown in Fig. 8(a-b), for CR1 and CR2, the martensitic structure is mainly martensite laths grouped in packets as the material is a medium-carbon steel [24–26]. For CR3 and CR4, a large amount of needle-like microstructure is clearly visible, indicated by the white and black arrows in Fig. 8(c-d). These structures are similar to martensite plates which usually occur in high-carbon steels, above 0.6 wt. % [25]. This suggests that an increase of carbon content in the remaining untransformed austenite takes place during transformation.

One simple method to estimate the carbon content in the austenite is to relate it to the M_s [27–29]. Such approach is possible using the following equation proposed in Ref [28]:

$$M_s(K) = 273 + 545.8\, e^{-1.362\, w_C}$$

where, w_C represents the carbon concentration in the austenite. With the values of the parameters collected by modeling the dilatation results and reported in Table 1, the second stage would correspond to the transformation from the carbon enriched austenite, therefore values from the parameters of the sigmoid sub-equation. In this case, the CM_s2 representing the calculated martensite start temperature of the second stage is to be used to estimate the carbon content at that precise moment. The calculated results for all 4 cooling rates are plotted in Fig. 9. The increase in carbon content is rather significant with 0.58%, 0.70%, 0.82% and 1.02% for CR1,

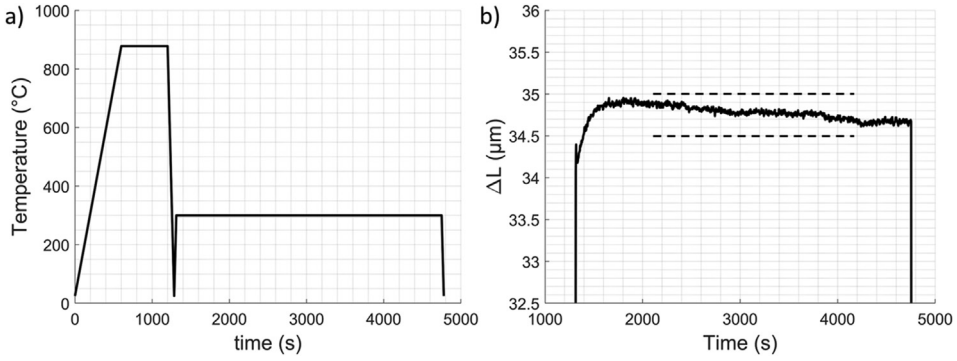

Fig. 10 – (a) Thermal cycle to determine the volume loss due to the effect of auto-tempering. The duration of tempering was chosen to be longer than the cooling duration of CR4. (b) Dilatation results for the interval of tempering of the previously shown thermal cycle.

CR2, CR3 and CR4 respectively. The high amount of carbon content in CR3 and CR4 explains the microstructure previously identified. It is also important to note that despite the presence of a CM_s2 and an increase in carbon content for CR1, the majority of the transformation occurs during the first phase as shown with the single reverse S shape in Fig. 3(a).

4. Discussion

In contrast to various modified K-M equations provided in the literature to model athermal martensitic transformation, the present equation addresses the complication of having more than one martensitic transformation. The acceleration and deceleration observed could be due to multiple mechanisms. Firstly, the prior austenite grain size is known to affect the M_s [11,30]. However, in the present study, all the samples had a similar average grain size of 22 μm at room temperature and therefore, this factor was dismissed from the analysis.

The acceleration and deceleration is best explained by considering the auto-tempering of martensite formed from initial austenite blocks, also referred as massive austenite blocks [17,31]. It implies the diffusion of carbon from the supersaturated martensite laths into the remaining or untransformed austenite [2,32]. This is also evidenced by the observed microstructures from Fig. 8 and the estimation of the carbon content from the modeling of the dilatation results from Fig. 9.

The carbon enrichment contributes to the stability of the untransformed austenite and therefore lowers the M_s [10,33,34]. A higher degree of undercooling would then be necessary in order to reach the new M_s for the transformation to continue further. The formation of the inflection point could then be explained by relating between the M_s variation and the cooling rate. For CR1, as the cooling rate is high, carbon diffusion was unable to occur at a sufficiently high rate to slow down the transformation. For CR2 and CR3, carbon diffusion from the initial fraction of martensite to the remaining austenite was able to lower the M_s at a higher rate than the cooling rate. Thus resulting in a M_s lower than the actual temperature which slows the transformation. In comparison to CR4 with a much slower cooling rate, the first stage has a high fraction of transformed martensite. This is due to the fact that with a lower cooling rate, the initial fraction of transformed martensite is also small, meaning that a lower amount of carbon atoms are able to diffuse to the remaining austenite. The M_s would then only slightly decrease. The deceleration does eventually happen when a larger amount of martensite is transformed.

In addition to the austenite stability due to carbon diffusion, a second concurrent effect of auto-tempering is the volume loss which directly correlates to the length decrease measured by dilatometry [35]. The possible influence of martensite auto-tempering was validated in the present study by performing a quench and tempering cycle, as shown in Fig. 10(a). It is assumed that after the quench, the microstructure is fully martensitic. The total sample length change for the selected interval of tempering was about 0.5 μm, as shown in Fig. 10(b). The obtained results clearly reveal that, the length change due to volume loss is not significant and unable to totally explain the martensitic transformation behavior.

5. Summary

Through the use of dilatometry, the different cooling rates below Ms revealed a two-stage martensitic transformation. The commonly used K-M equation to model the fraction of martensite as a function of temperature was unable to accurately predict the transformation and a new equation was therefore proposed. This new equation demonstrated a good capability to model the transformation. The second stage transformation was related to the carbon enrichment of austenite from the auto-tempering effect. This has been consistent with the findings from the microstructures which consist of martensite laths for fast cooling rates and martensite plates.

Declaration of Competing Interest

The authors declare that they have no known competing financial interests or personal relationships that could have appeared to influence the work reported in this paper.

Acknowledgements

This financial support from the Natural Sciences and Engineering Research Council of Canada (NSERC), the Metal Transformation Research and Innovation Consortium of Quebec (CRITM), Safran Landing Systems and Finkl Steel in the framework of an Industry-University Collaborative Research project (CRD 536717) is much appreciated. The authors are also thankful to Dr. R. Billlardon and J-S. Lemyre-Baron for the stimulating discussions.

REFERENCES

[1] Totten GE. Steel heat treatment handbook. Boca Raton, FL: Taylor & Francis; 2007.
[2] Seo EJ, Cho L, De Cooman BC. Modified methodology for the quench temperature selection in quenching and partitioning (Q&P) processing of steels. Metall Mater Trans 2016;47:3797–802.
[3] van Bohemen SMC, Sietsma J. The kinetics of bainite and martensite formation in steels during cooling. Mater Sci Eng, A 2010;527:6672–6.
[4] Fredj EB, Nanesa HG, Shahriari D, Morin J-B, Jahazi M. Effect of cooling rate on phase transformation and microstructure evolution in a large size forged ingot of medium carbon low alloy steel. In: TMS 2017 146th annual meeting & exhibition supplemental proceedings; 2017. p. 413–23.
[5] Bojack A, Zhao L, Morris PF, Sietsma J. In-situ determination of austenite and martensite formation in 13Cr6Ni2Mo supermartensitic stainless steel. Mater Char 2012;71:77–86.
[6] Obasi G, Pickering EJ, Vasileiou AN, Sun YL, Rathod D, Preuss M, et al. Measurement and prediction of phase

transformation kinetics in a nuclear steel during rapid thermal cycles. Metall Mater Trans 2019;50(4):1715–31.
[7] Escobar JD, Faria GA, Maia EL, Oliveira JP, Boll T, Seils S, et al. Fundamentals of isothermal austenite reversion in a Ti-stabilized 12Cr – 6 Ni – 2 Mo super martensitic stainless steel: thermodynamics versus experimental assessments. Acta Mater 2019;174:246–59.
[8] Escobar JD, Faria GA, Wu L, Oliveira JP, Mei PR, Ramirez AJ. Austenite reversion kinetics and stability during tempering of a Ti-stabilized supermartensitic stainless steel: correlative in situ synchrotron x-ray diffraction and dilatometry. Acta Mater 2017;138:92–9.
[9] Conde FF, Escobar JD, Oliveira JP, Jardini AL, Bose Filho WW, Avila JA. Austenite reversion kinetics and stability during tempering of an additively manufactured maraging 300 steel. Add Manuf 2019;29.
[10] van Bohemen SMC, Sietsma J. Kinetics of martensite formation in plain carbon steels: critical assessment of possible influence of austenite grain boundaries and autocatalysis. Mater Sci Technol 2014;30:1024–33.
[11] Celada Casero C, Sietsma J, Santofimia MJ. The role of the austenite grain size in the martensitic transformation in low carbon steels,. Mater Des 2019;167:107625.
[12] Guo YB, Sui GF, Liu YC, Chen Y, Zhang DT. Phase transformation mechanism of low-carbon high strength low alloy steel upon continuous cooling. Mater Res Innovat 2015;19. S8–S416-S8-422.
[13] Loewy S, Rheingans B, Meka SR, Mittemeijer EJ. Unusual martensite-formation kinetics in steels: observation of discontinuous transformation rates. Acta Mater 2014;64:93–9.
[14] Villa M, Pantleon K, Reich M, Kessler O, Somers MAJ. Kinetics of anomalous multi-step formation of lath martensite in steel. Acta Mater 2014;80:468–77.
[15] Liu C, Liu Y, Zhang D, Yan Z. Research on splitting phenomenon of isochronal martensitic transformation in T91 ferritic steel. Phase Transitions 2012;85:461–70.
[16] T. American Society for, Materials. ASTM E975-13 : standard practice for X-Ray determination of retained austenite in steel with near random crystallographic orientation. Pennsylvania: ASTM, Philadelphia; 2013.
[17] Caballero FG, Álvarez LF, Capdevila C, Garcıa de Andrés C. The origin of splitting phenomena in the martensitic transformation of stainless steels. Scr Mater 2003;49(4):315–20.
[18] Khan SA, Bhadeshia HKD. Kinetics of martensitic transformation in partially bainitic 300M steel. Mat Sci Eng A 1990;129(2):257–72.
[19] Yi HL, Lee KY, Bhadeshia HKDH. Mechanical stabilisation of retained austenite in -TRIP steel. Mat Sci Eng A Mat Sci Eng A 2011;528(18):5900–3.
[20] Koistinen DP, Marburger RE. A general equation prescribing the extent of the austenite-martensite transformation in pure iron-carbon alloys and plain carbon steels,. Acta Metall 1959;7:59–60.
[21] Gür CH, Şimşir C. Simulation of quenching: a review. Mat Perf Char 2012;1:1–37.
[22] Mustak O, Evcil E, Simsir C. Simulation of through-hardening of SAE 52100 steel bearings – Part I: determination of material properties. Materialwissenschaft und Werkstofftechnik 2016;47:735–45.
[23] Bhadeshia HKDH. Multiple, simultaneous, martensitic transformations: implications on transformation texture intensities. Mater Sci Forum 2013;762:9–13.
[24] Krauss G, Marder AR. The morphology of martensite in iron alloys. Metall Trans Metall Trans 1971;2(9):2343–57.
[25] Stormvinter A, Borgenstam A, Hedstrom P. Investigation of lath and plate martensite in a carbon steel. Solid State Phenomena 2011;172-174:61–6.
[26] Vander Voort G. Microstructure of Ferrous Alloys 2001;68:28–34.
[27] Talebi SH, Jahazi M, Melkonyan H. Retained austenite decomposition and carbide precipitation during isothermal tempering of a medium-carbon low-alloy bainitic steel. Materials (Basel) 2018;11(8).
[28] Wang J, Van Der Zwaag S. Stabilization mechanisms of retained austenite in transformation-induced plasticity steel. Metall Mat Trans A 2001;32(6):1527–39.
[29] van Bohemen SMC. Bainite and martensite start temperature calculated with exponential carbon dependence. Mater Sci Technol 2013;28(4):487–95.
[30] Lee S-J, Van Tyne CJ. A kinetics model for martensite transformation in plain carbon and low-alloyed steels. Metall Mater Trans 2011;43:422–7.
[31] García de Andrés C, Caballero FG, Capdevila C, Álvarez LF. Application of dilatometric analysis to the study of solid–solid phase transformations in steels. Mater Char 2002;48:101–11.
[32] Ooi SW, Cho YR, Oh JK, Bhadeshia HKDH. Carbon enrichment in residual austenite during martensitic. Int Conf Mart Transf (ICOMAT) 2010:179–85.
[33] Morgan ER, Ko T. Thermal stabilization of austenite in iron-carbon-nickel alloys. Acta Metall 1953;1:36–48.
[34] Hsu TY. Carbon diffusion and kinetics during the lath martensite formation. Le Journal de Physique IV 05 1995;5(8):351–4.
[35] Jung M, Lee S-J, Lee Y-K. Microstructural and dilatational changes during tempering and tempering kinetics in martensitic medium-carbon steel. Metall Mater Trans 2009;40:551–9.